Society of Exploration Geophysicist, International Exposition and Sixty Eighth Annual Meeting, September 13 - 18, 1998, Expanded Abstracts, pp. 338-341.

Microseismic mapping of a Cotton Valley hydraulic fracture using decimated downhole arrays

J.T. Rutledge [*], Nambe Geophysical, Inc., W.S. Phillips and L.S. House, Los Alamos National Laboratory, and R.J. Zinno, Union Pacific Resources Company

Summary

An extensive microseismic data set was collected during three hydraulic fracture operations in the Cotton Valley gas field of East Texas. Two 48-level, 3-component geophone arrays were deployed. We have mapped the microseismicity of the Stage 2 completion interval using data from 9 or fewer geophone stations. Gross fracture dimensions obtained from the 9-station data were the same as determined from the full-array data. Seismic velocities and station corrections were estimated via a joint hypocenter-velocity inversion. Master-event relative mapping applied to the most populous cluster of located seismicity improved location precision 10-fold and resolved a 150-ft-length, horizontal linear feature with width and depth dimensions of less than 10 ft. The linear cluster lies near the upper boundary of the treatment interval and implies that the majority of mapped seismicity is constrained to about 4% of the total injection depth interval. Fine-scale temporal growth patterns were revealed as well.

Introduction

Downhole detection and mapping of microearthquakes induced during hydraulic fracturing currently promises the best combination of resolution, coverage and economy for imaging stimulated fracture geometry (several methods and studies are summarized by Phillips et al., 1996). In May, 1997 a consortia of operators and service companies conducted an extensive hydraulic fracture imaging demonstration in the Cotton Valley gas field of East Texas (Walker, 1997). The Cotton Valley Project was an important test of the microseismic technique in a tight-gas sand reservoir at interwell distances typically found in this production environment (>1000 ft). Well completions and re-completions in tight-gas sand reservoirs account for many of the hydraulic-fracture operations conducted in the United States, and, therefore, constitute a large potential application of the microseismic imaging technique. The commercial viability of the technique will strongly depend on the effectiveness of low-cost applications in this production environment. Our objective is to demonstrate the level of detail to which a hydraulic fracture can be imaged using microearthquake data recorded by arrays that might be available in typical, commercial applications. Using station-decimated versions of the full array data, we show examples of velocity calibration, absolute source mapping and high-precision fracture imaging via relative source mapping.

Data

Details of the geology, fracture design, instrumentation, deployment and data acquisition are described in Walker (1997). Two 2350-ft-length, 48-level, 3-component geophone arrays were cemented behind the casing of two offset monitor wells (Figure 1). Sonde spacing was 50 ft. Signals were amplified 60 dB downhole; an additional 48 dB of gain was applied uphole before digitizing at a 1 msec sample interval.

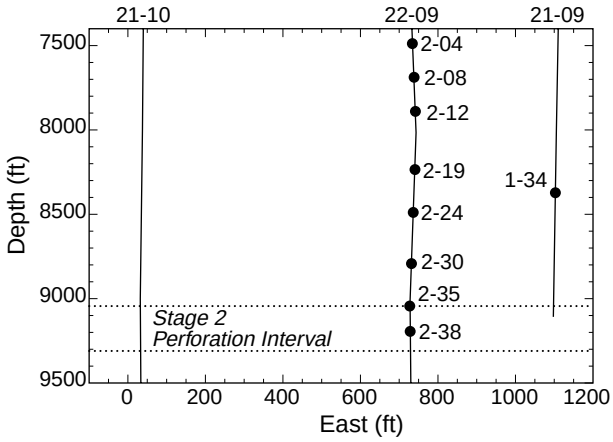

Fig. 1: Geophone stations used in the decimated-array mapping. Well 21-10 is the treatment well. 22-09 and 21-09 are the monitor wells. A map view of these wells can be seen in Figure 2.

Three stages of hydraulic fracture treatment were monitored in the Cotton Valley formation (Walker, 1997). We have analyzed the microseismicity from the Stage 2 treatment, a 6900 barrel (1100 m^3) injection over the perforated depth interval 9044 to 9310 ft. Nearly 1200 events were detected. We picked P- and S-arrivals on 9 stations (Figure 1). The largest 620 events were examined, and, of these, arrivals on multiple stations could be identified and reliably picked on 380 events. From the 9-station data, we can further decimate to demonstrate the mapping capability of various receiver configurations that would mimic low-cost deployments, such as a 5-level retrievable array in a single well (well 22-09, Figure 1). The benefits of adding a single-level receiver in a second monitor well can also be easily demonstrated (well 21-09, Figure 1).

Velocity calibration

Seismic velocities and station time corrections were estimated via a joint hypocenter-velocity inversion routine (Phillips et al., 1996). Input data included 9 primacord shots fired within or just

outside the Stage 2 depth interval of the treatment well and the 71 highest quality microearthquakes in which P and S arrivals were identified on all 9 stations and at least 2 hodograms were available. Including hodogram data helps resolve trade-off between velocities and hypocenters in multiple-well data. The shots used have travel paths similar to the microearthquake data. Perforation shots preceding completion treatments can be used similarly for calibration. Shot origin times were obtained from a geophone placed in the cable head of the wireline shot assembly.

We solved for homogeneous Vp and Vs and station time corrections for P and S arrivals. The station corrections for the deepest, closest receiver (2-38) were fixed at zero to constrain trade-off between velocity and station corrections. Origin times and P arrivals on all 9 stations of the shots could be very reliably picked; poorer quality S arrivals could be observed on only a few of these shot records. Initially we solved for Vp and P-arrival-time corrections using the P-wave shot data alone. We then ran the inversion again to solve for Vs and the S-arrival-time corrections, using the shot data supplemented by the 71 highest quality microearthquake data. The prior-determined Vp and P-time corrections were input as fixed parameters in the second-run inversion. P-arrival station corrections show a clear trend of delays increasing upward with steepening inclination of raypaths, a trend that may be primarily due to the transverse-isotropy effect of layering.

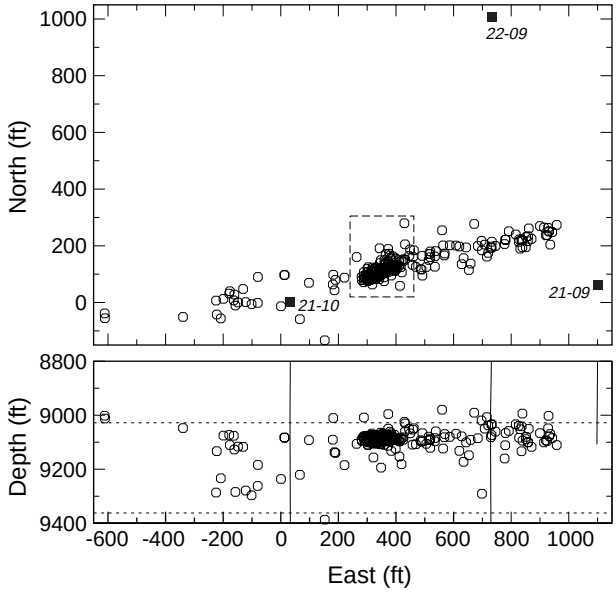

Fig. 2: Map and depth views of hypocenters determined from the 9-station data. The dashed box encloses an event cluster selected for master-event, relative mapping (Figures 3 and 4).

Location of 287 events with RMS travel-time residuals less than 2 msec were determined using the final velocity model and the 9-station data (Figure 2). Fracture orientation, length and height are essentially identical to that obtained using the full array data (Walker, 1997). Error ellipsoids are flat lying, trending along strike of the seismicity, with 50 ft length major axes; depth error is about ±10 ft.

Detailed structure resolution using relative mapping

High-precision fracture images can be obtained by locating events relative to a master event location. Earthquakes that occur repeatedly on the same fault plane or along adjacent, similarly-oriented fault planes will produce nearly identical waveforms at a given receiver if they result from the same sense of slip. The relative location technique is based on grouping such similar waveforms with the objective of illuminating repeatedly activated structures. Relative arrival times are obtained by consistently picking on easily identified peaks or troughs (e.g. Phillips et al., 1997) or by cross-correlation (e.g. Moriya et al., 1994). Precision of the relative picks is greatly improved from the more subjective picks of P-and S-wave onsets. The grouped events are then mapped relative to a master event using the relative P-P and S-S times. By using the relative arrival time data, velocity uncertainties and other path effects are effectively removed over the greater portion of the clustered events' common source-receiver paths. The resultant event cluster geometry is fairly insensitive to reasonable uncertainty in the near-source velocities.

We applied relative mapping to a group of 161 events that fall in a tight cluster about 400 ft east of the treatment well (56% of the located events, Figure 2) using travel time data from 6 receivers (2-38 to 2-19 in well 22-09 and 1-34 in well 21-09, Figure 1). Absolute locations using original picks show a planar feature striking N70E and dipping 45° SE (Figure 3). After obtaining the relative arrival times and applying the master-event location technique, the event locations form a well-defined, horizontal line (Figure 4). The main group of events is separate from a secondary group, and was distinguished by a change in the S waveform character at station 2-35 (solid and open symbols, respectively, Figure 4). The secondary events also fall slightly deeper. Error ellipsoids were reduced 10-fold with major axes lengths of only 6 ft, oriented along strike.

Fracture growth patterns

Fracture growth patterns are revealed by the temporal behavior of the relocated events. The event cluster was activated repeatedly during different injection phases; the initial activation sequence is shown in Figure 5. Diameters of the circles are proportional to the log of peak amplitudes (a pseudo-magnitude scale). The seismicity, at least initially, migrates east to west toward the injection well. At the eastern end of the cluster there is a repeated, small-to-big-to-small event sequence among 3 sub-clusters. Within each sub-cluster, similar sized events occur and also appears to migrate westward. The sub-clusters may represent discrete, isolated fractures along the overall seismicity trend, with event sizes within each

Mapping of a Cotton Valley hydraulic fracture

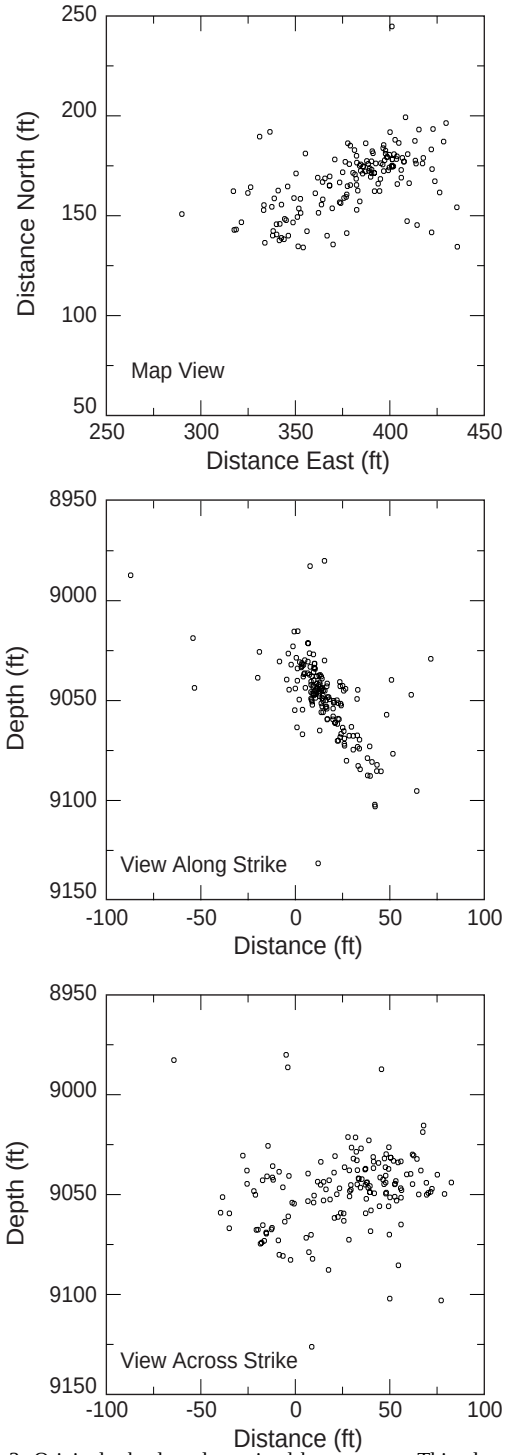

Fig. 3: Original, absolute-determined hypocenters. This cluster is also outlined in Figure 2. The map-view distances (top) are with respect to the treatment well (Figure 2).

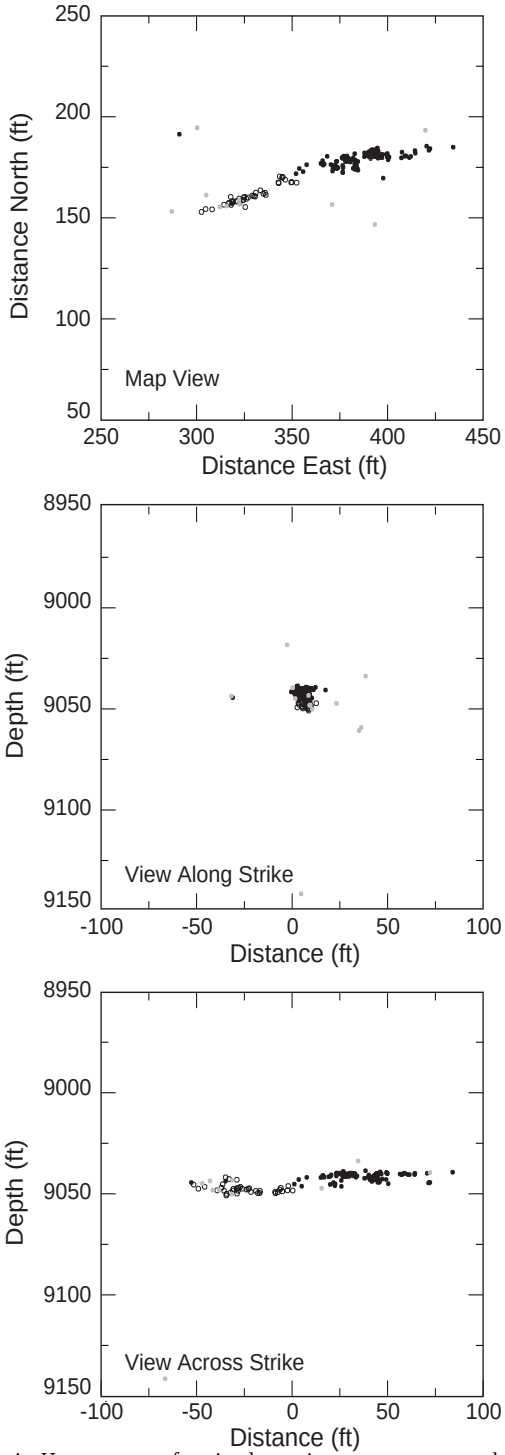

Fig. 4: Hypocenters after implementing master-event, relative mapping technique. Solid and open symbol events were distinguished by a change in the S-waveforms character at station 2-35 and are spatially distinct.

sub-cluster being limited by fracture dimension. Associating source dimension estimates with the temporal cluster patterns should further aid in interpreting and characterizing the growth patterns of the injection-induced seismicity throughout the treatment. In general, the repetitive, detailed spatial-temporal patterns revealed further support the precise geometry resolved by the relative-mapping method.

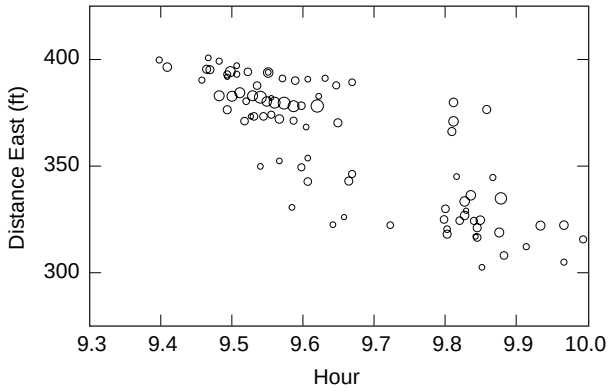

Fig. 5: Temporal sequence of the remapped cluster of Figure 4. Hypocenter positions east of the treatment well are plotted versus time. Circle diameters are proportional to event magnitude. This is the initial activation of the cluster. Event locations migrate east to west toward the treatment well. At the eastern end of the cluster there is a repeated, small-to-big-to-small event sequence among 3 sub-clusters. Within each of these 3 sub-clusters events also migrate westward.

Conclusions

Decimated-array mapping of the Stage 2 Cotton Valley microseismic data provided the same gross fracture dimensions obtained using the full array data. Relative mapping applied to the most populous cluster of seismicity improved location precision 10-fold and resolved a 150-ft-length, horizontal linear feature with width and depth dimensions of less than 10 ft. The cluster lies near the upper boundary of the treatment interval and implies that the majority of mapped seismicity is constrained to about 4% of the total injection depth interval (266 ft). This tube-like geometry of injection-induced seismicity is similar to a feature resolved by House et al. (1996) from a subset of microearthquake data collected during a waste injection operation in the Frio Formation, East Texas (Keck and Withers, 1994). Fine-scale temporal patterns of the clustered seismicity show repeated sequences of events migrating toward the injection well.

Acknowledgment

We thank Robert Withers and Robert Dart of ARCO Exploration and Production Technology for providing the data. Much of the accessory log and survey data were compiled by Paul Branagan and Richard Peterson of Branagan and Associates. These analyses were supported by the U.S. Department of Energy's Natural Gas and Oil Technology Partnership.

References

House, L., Flores, R. and Withers, R., 1996, Microearthquakes induced by a hydraulic injection in sedimentary rock, East Texas: Soc. Explor. Geophys. 66th Annual Meeting., Extended Abstracts, 110-113.

Keck, R.G. and Withers, R.J., 1994, A field demonstration of hydraulic fracturing for solid waste injection with real-time passive seismic monitoring: SPE paper 28495, presented at 69th Soc. Petro. Eng. Annual Technical Conference and Exhibition, New Orleans, Louisianna.

Moriya, H., Nagano, K., and Niitsuma, H., 1994, Precise source location of AE doublet by spectral matrix analysis of triaxial hodogram: Geophysics, 59, 36-45.

Phillips, W.S., House L.S., and Fehler, M.C., 1997, Detailed joint structure in a geothermal reservoir from studies of induced microearthquake clusters: J. Geophys. Res., 102, 11745-11763.

Phillips, W.S., Rutledge, J.T., Fairbanks, T.D., Gardner, T.L., Miller, M.E., Schuessler, B.K., 1996, Reservoir fracture mapping using microearthquakes: Austin Chalk, Giddings Field, TX and 76 Field, Clinton Co., KY: SPE Paper 36651, presented at the 1996 Soc. Petro. Eng. Annual Technical Conference and Exhibition, Denver, Colorado.

Walker, Jr., R.N., 1997, Cotton Valley Hydraulic Fracture Imaging Project: SPE paper 38577, presented at the 1997 Soc. Petro. Eng. Annual Technical Conference and Exhibition, San Antonio, Texas.